Nanoscale

COMMUNICATION

High-yield synthesis and optical properties of g-C_3N_4†

Cite this: DOI: 10.1039/c5nr02905h

Received 4th May 2015,
Accepted 19th June 2015

DOI: 10.1039/c5nr02905h

www.rsc.org/nanoscale

Yanwen Yuan,[a] Lulu Zhang,[a] Jun Xing,[a] M. Iqbal Bakti Utama,[a] Xin Lu,[a] Kezhao Du,[a] Yongmei Li,[b] Xiao Hu,[b] Shijie Wang,[c] Aziz Genç,[d] Rafal Dunin-Borkowski,[e] Jordi Arbiol[d,f] and Qihua Xiong*[a,g]

Graphitic carbon nitride (g-C_3N_4), a metal-free semiconductor with a band gap of 2.7 eV, has received considerable attention owing to its fascinating photocatalytic performances under visible-light. g-C_3N_4 exhibits high thermal and chemical stability and non-toxicity such that it has been considered as the most promising photocatalyst for environmental improvement and energy conservation. Hence, it is of great importance to obtain high-quality g-C_3N_4 and gain a clear understanding of its optical properties. Herein, we report a high-yield synthesis of g-C_3N_4 products *via* heating of high vacuum-sealed melamine powder in an ampoule at temperatures between 450 and 650 °C. Using transmission electron microscopy (TEM), scanning transmission electron microscopy (STEM), electron energy loss spectroscopy (EELS), thermogravimetric analysis (TGA), X-ray diffraction (XRD), and X-ray photoelectron spectroscopy (XPS), the chemical composition and crystallization of the as-produced g-C_3N_4 are demonstrated. A systematic optical study of g-C_3N_4 is carried out with several approaches. The optical phonon behavior of g-C_3N_4 is revealed by infrared and Raman spectroscopy, and the emission properties of g-C_3N_4 are investigated using photoluminescence (PL) spectroscopy, while the photocatalytic properties are explored by the photodegradation experiment.

Introduction

Graphitic carbon nitride (g-C_3N_4), one of the carbon nitride allotropes, has a graphene-like layered structure composed of heptazine units and the bridge amino groups. With a bandgap of 2.7 eV, g-C_3N_4 exhibits outstanding photocatalytic performance in various photochemical reactions, such as in photodegradation and photocatalytic water splitting under visible light.[1–5] Unlike traditional organic semiconductors, g-C_3N_4 has excellent thermal and chemical stability, and it is also pollution-free, earth-abundant, inexpensive and facile to produce.[6] Therefore, g-C_3N_4 is a very competitive candidate for depollution and solar energy development. The high-quality preparation and optical properties of g-C_3N_4 are thus of sustained interest.[7]

Great efforts were made to obtain high quality g-C_3N_4 in previous literature.[8–10] High-yield synthesis of nano-sized g-C_3N_4 from bulk g-C_3N_4 has been reported recently as well.[11] However, the most commonly used approach for the bulk g-C_3N_4 preparation is still by heating the reagent in air, such as cyanamide, dicyandiamide, or melamine.[12,13] This one-step method is simple and easy to control; however, it suffers from a very low yield (~6%) because the polymerization temperature of g-C_3N_4 is higher than the sublimation point of the reagent, causing the reagent loss before the reaction occurs.[14] On the other hand, air contains many gas components such as oxygen and nitrogen, so there may be oxidation or other unexpected reactions during the heating process. To solve the problem on purity and yield, we choose to synthesize g-C_3N_4 in a vacuum-sealed environment.[15,16] In this paper, all reagents are sealed inside an evacuated ampoule at a pressure of 3–10 mbar and then heated to the targeted reaction temperature. Since the reagent is not able to escape from the sealed ampoule, a high yield production of g-C_3N_4 (~61%) is achieved. Additionally, there is negligible contamination or oxidation of the g-C_3N_4

[a]*Division of Physics and Applied Physics, School of Physical and Mathematical Sciences, Nanyang Technological University, 637371, Singapore. E-mail: Qihua@ntu.edu.sg*
[b]*School of Materials Science and Engineering, Nanyang Technological University, 639798, Singapore*
[c]*Institute of Materials Research & Engineering, Agency for Science, Technologies and Research, 3 Research Link, 117602, Singapore*
[d]*Institut de Ciència de Materials de Barcelona, ICMAB-CSIC, Campus de la UAB, 08193 Bellaterra, Spain*
[e]*Ernst Ruska-Centre for Microscopy and Spectroscopy with Electrons and Peter Grünberg Institute, Forschungszentrum Jülich GmbH, D-52425 Jülich, Germany*
[f]*Institució Catalana de Recerca i Estudis Avançats, ICREA, Passeig Lluís Companys, 23, 08010 Barcelona, Spain*
[g]*NOVITAS, Nanoelectronics Centre of Excellence, School of Electrical and Electronic Engineering, Nanyang Technological University, 639798, Singapore*

†Electronic supplementary information (ESI) available: (1) STEM-HAADF, STEM-EELS and XRD result of the hydrogen-bonded sample. (2) Raman and IR peak positions and their related modes and descriptions of vibration. (3) The Gaussian fitting of PL emission spectra of the g-C_3N_4 sample. (4) PL emission spectra of the g-C_3N_4 products in water. See DOI: 10.1039/c5nr02905h

products since the heating process is performed in a vacuum. With TEM, STEM-EELS, TGA, XRD and XPS, the composition and structure of the as-produced g-C_3N_4 are characterized to demonstrate the good quality g-C_3N_4 produced *via* our synthesis approach.

Optimizing the optical properties of g-C_3N_4 is also of great importance to achieve better performance in photocatalytic reactions. As revealed by the state-of-the-art optical studies of g-C_3N_4, different heating temperatures of carbon nitride may lead to the change in the chemical structure of the sample.[17,18] A blue- or red-shift of the photoluminescence may also occur.[1,19–21] Following these studies, we obtained a series of products at various heating temperatures and carried out optical characterization including infrared, Raman, and PL spectroscopy to reveal the phonon behavior and the chemical bonds of the g-C_3N_4 products. We also observe a tunable PL emission in the g-C_3N_4 products processed at different temperatures and attribute this phenomenon to the extension of the g-C_3N_4 network at increasing temperature. Moreover, a photocatalytic decomposition experiment using g-C_3N_4 products is demonstrated, corroborating the excellent photocatalytic properties of the g-C_3N_4 products.

Experimental section

Materials synthesis

50 mg of melamine powder were firstly sealed in a quartz ampoule with a diameter of 13 mm and a length of 6–8 cm, after which the ampoule was pumped down to 3–10 mbar. Then, the ampoule is placed in the central region of a quartz tube furnace and heated at a ramp-up rate of 8 °C min^{-1} to the designated temperatures between 450 and 650 °C. The temperature is then held constant for 2 hours. The ampoule was taken out after cooling to room temperature and opened by using a glass cutter. The powders inside the ampoule were collected into a 2 ml centrifuge tube and ultrasonicated in deionized water before dispersion. After 10 min centrifugation at the rate of 14 650 rpm, the supernatant liquid was discarded. This washing process is repeated 5 times to remove the unreacted melamine. After washing, the powder is dried in an oven at 60 °C for 3–5 hours.

Characterization methods

TEM characterization. The g-C_3N_4 products are dispersed in isopropyl alcohol by ultrasonication and then deposited on a lacey carbon TEM grid. The morphology of the g-C_3N_4 products was observed by transmission electron microscopy (JEOL JEM 1400) with an accelerating voltage of 100 kV.

STEM-EELS characterization. The STEM-EELS studies of the g-C_3N_4 products were conducted by using a FEI Titan microscope operated at 80 kV under a high angle annular dark field (HAADF).

TGA measurements. The weight percent of each composition of the g-C_3N_4 products was determined by TGA (TA Instruments Q500) with a sampling rate of 10 °C min^{-1} at 800 °C in air.

XRD measurements. XRD of the g-C_3N_4 products was performed using a Bruker D8 powder X-ray diffractometer with Cu Kα radiation (1.54056 Å) and a sampling rate of 0.8 degrees per min.

XPS measurements. To study the chemical bond of the g-C_3N_4 products, XPS measurements were performed on a VG ESCALAB 220i-XL system using a monochromatic Al Kα source. The pass energy of the analyzer was set at 10 eV to have a high measurement resolution. The XPS binding energy scale was calibrated with pure Au, Ag, and Cu standard samples by setting the Au 4f7/2, Ag 3d5/2, and Cu 2p3/2 peaks at binding energies of 83.98 ± 0.02 eV, 368.26 ± 0.02 eV, and 932.67 ± 0.02 eV, respectively. The binding energy calibrations were made against the C 1s peak to eliminate the charging of the sample during analysis.

Optical property studies

Fourier transform infrared spectroscopy (FTIR). FTIR (Perkin Elmer Frontier) is used to determine the chemical structure and the optical properties of the products by scanning from 600 cm^{-1} to 4000 cm^{-1} 16 times.

Raman spectroscopy. Raman scattering spectroscopy measurements were carried out with 785 nm excitation using a micro-Raman spectrometer (Horiba-JY T64000). The laser power is about 0.3 mW and the measurements were conducted in triple mode with 1800 g mm^{-1} grating.

Photoluminescence spectroscopy. The photoluminescence properties were investigated using a micro-Raman spectrometer (Horiba-JY T64000) in the backscattering configuration excited using a He Cd laser (325 nm) with a power intensity of 0.3 mW (single mode, 600 g mm^{-1} grating). The liquid nitrogen continuous flow cryostat (Cryo Industry of America, USA) was used to provide a continuous temperature variation from 77 to 300 K.

Photocatalytic degradation experiment

10 mg l^{-1} methylene blue and 1 g l^{-1} g-C_3N_4 products were used in the experiment and mixed at a stirring rate of 800 rpm in the dark for 30 min. Then the mixture was moved to the solar simulator for photocatalytic experiment at the same stirring rate. After each designated interval time (5 min, 5 min, 10 min, 10 min, 20 min, 20 min, 40 min), 1 mL sample is collected into a 2 ml centrifuge tube and centrifuged for 10 min at the rate of 14 650 rpm. Then, the UV-VIS absorption spectra of the supernatant liquid were recorded using a Lambda 950 spectrophotometer at room temperature.

Results and discussion

Preparation and characterization of high-yield g-C_3N_4 products

The formation of a highly crystalline carbon nitride usually follows the self-condensation process of cyanamide, dicyandiamide, or melamine during heating.[22–24] In our case, we use

melamine as the reagent in a sealed quartz ampoule. The vacuum level inside the ampoule is controlled under 3–10 mbar. With a heating ramp-up rate of 8 degree centigrade per minute, the ampoules were heated at different temperatures (450, 500, 550, 600, and 650 °C) for 2 hours.

As previous literature indicated,[25] the melamine will first form melem (an intermediate product during self-condensation of melamine) which is then polymerized into a g-C_3N_4 network, accompanied by a color change from white (melamine, melem) to yellow (g-C_3N_4). This phenomenon was also observed in our g-C_3N_4 products heated at different temperatures. Fig. 1(a) shows the photograph of all the products synthesized at different temperatures. The color of the products changes from white (450 °C) to pale yellow (500 °C), yellow (550 °C), brown (600 °C), and to dark brown (650 °C), which indicates that the composition of the products is changed. For the white color sample, the composition should be melem in majority. The yellower the sample becomes, the more g-C_3N_4 it contains. When the preparation temperature is too high (600–650 °C), the sample turns into brown and dark brown, which may be due to the carbonization of the sample at high temperatures.

Fig. 1(b–f) display the TEM images of the carbon nitride products processed at different temperatures. The morphology of products obtained at 450 °C and 500 °C have a unique rod-like structure, which we suspect to be the hydrogen-bonded framework of melem.[26] Beside the rods, there are also a few layered flakes with a width of several hundred nanometers in products obtained at 450 °C and 500 °C. When the preparation temperature is above 550 °C, the flakes became the main products and the average size also increased to several micrometers.

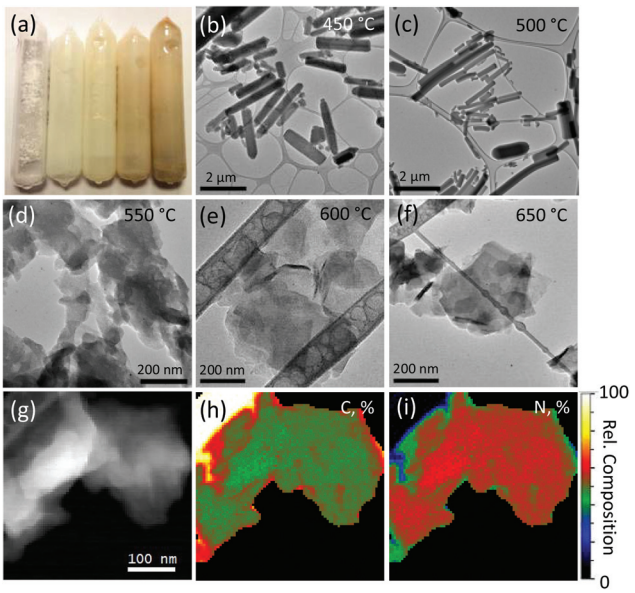

Fig. 1 (a) A photograph of the g-C_3N_4 products synthesized *via* the thermal condensation of melamine in a vacuum-sealed ampoule at different temperatures (from left to right: 450 °C, 500 °C, 550 °C, 600 °C, and 650 °C). (b–f) TEM images of the products synthesized *via* the thermal condensation of melamine at 450 °C to 650 °C. The scale bars of each figure are shown at the bottom. (g) STEM-HAADF micrograph obtained simultaneously during EELS acquisition from the g-C_3N_4 flakes within an area of 557 nm × 557 nm. (h, i) Relative compositions of C and N in the elemental mapping. The scale bars of panels (h, i) are the same as that of panel (g).

To figure out the composition of the rods and flakes, STEM-HAADF and STEM-EELS have been conducted. Fig. 1(g) shows the STEM-HAADF image of a flake obtained at 600 °C, and Fig. 1(h and i) show the EELS chemical composition maps for C and N, obtained from the flake. Chemical composition maps suggest a fairly homogeneous distribution of C and N throughout the flake. In general, the carbon nitride flake has a relative C composition of ~45 ± 1 at% and a relative N composition of ~55 ± 1 at%, which is almost equal to the nominal compositions of the C_3N_4 phase (C: 42.9%, N: 57.1%). Meanwhile, the EELS result from the bulk of the rod (Fig. S1†) also shows homogeneous distribution of C (~41 ± 0.5 at%) and N (~59 ± 0.5 at%). In this latest case, the C/N ratio is smaller than the nominal compositions of the C_3N_4 phase, suggesting a composition in good agreement with polymeric melem (C: 37.5–42.9%, N: 62.5–57.1%).

To confirm the content of the g-C_3N_4 products, we have conducted further characterization. Thermogravimetric analysis (TGA) was performed to find the weight percent of each composition of the heated products. All the samples were heated from room temperature to 700 °C at a rate of 10 °C min^{-1} in air, and the TGA curves are shown in Fig. 2(a). For the samples obtained at 450 °C and 500 °C, the weight loss at 100 °C for bound water (5–10%), 430 °C for melem (9–14%) and 550 °C for g-C_3N_4 (74–77%) was easily identified by their different temperatures of combustion or evaporation. Meanwhile, the samples obtained at 550–650 °C show a high purity of the g-C_3N_4 level (82–94%), which is in good agreement with the STEM-EELS results. We also observed the weight increase after 640 °C for the samples obtained at 550 °C–660 °C, and we suspect it might be due to the oxidation of the impurities. Considering the loss from the unreacted melamine, melem and impurities, we obtained 30.5 mg g-C_3N_4 from 50.0 mg melamine, so the highest yield of g-C_3N_4 can reach up to 61% when the heating temperature is 550 °C. Considering the theoretical yield of 73%, the reaction efficiency from melamine ($C_3N_6H_6$) to g-C_3N_4 is almost 84%, this high yield has not been achieved in previous work.

Fig. 2(b) shows the X-ray diffraction (XRD) patterns of both melamine and its heated products. As the preparation temperature increases, the melamine index peak was gradually eliminated. For all the heated products, a strong new peak at 27.4° appeared, representing the typical stacking structure of g-C_3N_4 layers in the (002) direction.[27–29] And for the samples obtained at 550 °C–650 °C, there are also few weaker XRD peaks at 13.0°, 44.5° and 57.5°, which represent the (100), (201) and (004) directions in the g-C_3N_4 crystal lattice separately.[30] In the case of samples obtained at 450 °C and 500 °C, there is another strong peak at 11.0°, which is the character-

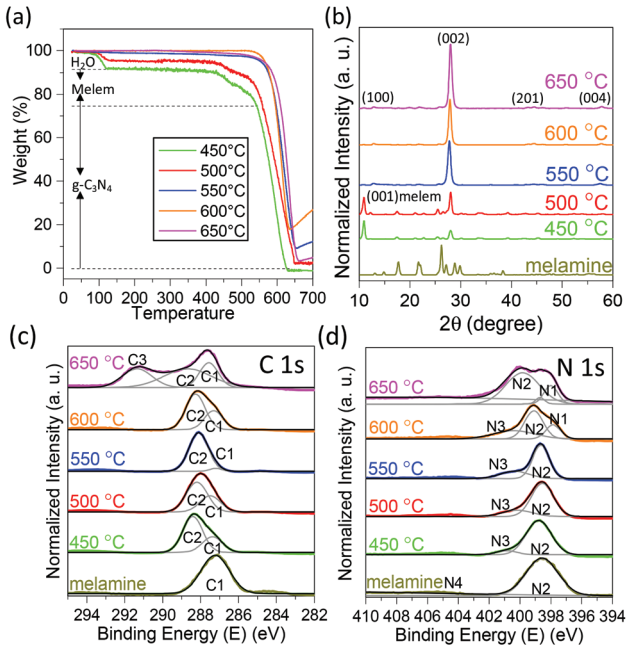

Fig. 2 (a) TGA result of the g-C_3N_4 products synthesized at different temperatures. The weight loss from room temperature to 100 °C is labelled as water and the weight loss from 100 °C to 450 °C is labelled as melem, meanwhile the weight loss from 450 °C to 625 °C is labelled as g-C_3N_4. (b) Experimental XRD curves of melamine and its heated products. The (100), (002), (201) and (004) directions in g-C_3N_4 crystal lattices have been labelled at 13.0°, 27.4°, 44.5° and 57.5° separately, meanwhile the (100) directions in melem crystal lattices have been labelled at 11.0°. (c, d) The normalized XPS spectra of the g-C_3N_4 products obtained at different temperatures: (c) C 1s spectrum and (d) N 1s spectrum.

istic peak of the hydrogen-bonded framework of melem.[26] This hydrogen-bonded framework is formed by the rearrangement of the melem molecules with the appearance of water, and its destruction can be achieved when the sample is heated above 100 °C (*i.e.*, the dehydration temperature of crystal water); consequently, the characteristic peak at 11.0° then disappears (ESI, Fig. S2†).

X-ray photoelectron spectroscopy (XPS) was conducted to determine the chemical bonding of the g-C_3N_4 products. In Fig. 2(c) and (d), the high-resolution C 1s and N 1s spectra of both melamine and the g-C_3N_4 products have been collected and then deconvolved into several Gaussian peaks. In the case of melamine, the C1 peak at 287 eV represents the sp^2 C atoms in the aromatic ring attached to the $-NH_2$ group.[31] After the self-condensation of melamine during annealing, the C1 peak disappeared because of deamination. Instead, the C2 peak originated from sp^2 C atoms bonded to N inside the aromatic structure, appeared at 288.5 eV.[32,33] Remarkably, when the heating temperature is above 600 °C, a C3 peak appears at 291 eV. Considering the carbonization of the sample at high temperatures, this peak probably comes from the carbon π–π* transition.[34] The N 1s spectra also show similar results. For melamine, the strong N2 peak at 399 eV represents the sp^2 N atoms involved in triazine rings.[35] Meanwhile, the N4 peak at 405 eV is contributed by the sp^3 N atoms in the amino groups. For the heated products, a new peak (N3 at 401 eV) shows up, which indicates the existence of the bridging sp^3 N atoms in $N–(C)_3$ after the reaction.[36] When the growth temperature is above 600 °C, a weak peak N4 at 398 eV appears. Coupled with the observations of C3 peaks from C 1s spectra, this peak can be assigned to pyridinic N atoms originated from the carbonization of g-C_3N_4.[37,38]

Fourier transform infrared spectroscopy (FTIR) and Raman studies of g-C_3N_4 products

To investigate the change in the chemical structure during thermal condensation and to gain insight into the optical properties of the g-C_3N_4 products, Fourier transform infrared spectroscopy (FTIR) and Raman spectroscopy were conducted on the samples. Fig. 3(a) shows the FTIR spectra of both melamine and the g-C_3N_4 products. For melamine, the peaks at 3472, 3417, and 3325 cm^{-1} are attributed to stretching and deformation modes of $–NH_2$ groups.[39] These peaks gradually decreased when the preparation temperature increases, indicating the process of deamination. Meanwhile, the peak at 807 cm^{-1}, which corresponds to the breathing mode of the triazine ring, remains.[40] There is also a bunch of peaks appearing in the 1100–1650 cm^{-1} region, which are related to the

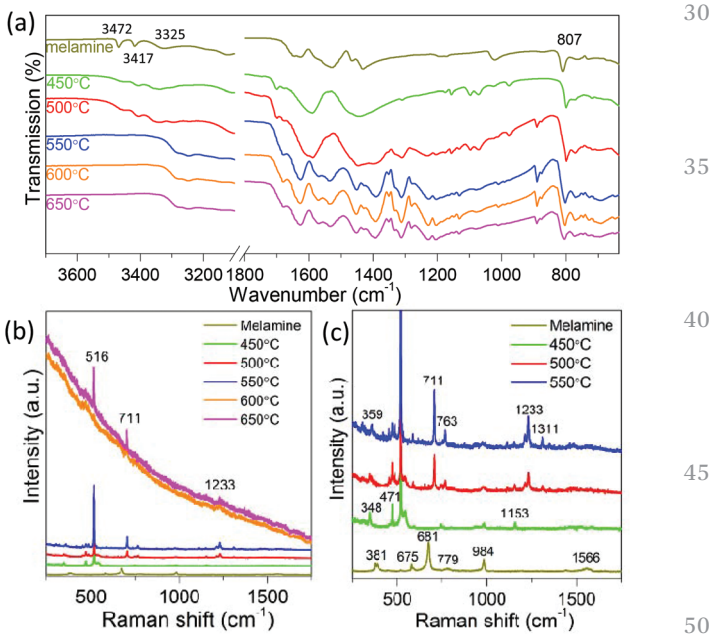

Fig. 3 (a) The FTIR spectra of the melamine and the g-C_3N_4 products obtained at different temperatures. (b) The Raman spectra of the g-C_3N_4 products obtained at different temperatures using the near-infrared (NIR 785 nm) light for excitation, in which peak at 516 cm^{-1} is from the silicon substrate, and peaks at 711 and 1233 cm^{-1} are the typical characterization peaks of g-C_3N_4. (c) The zoom-in view of Raman spectra of melamine and the g-C_3N_4 products obtained from 450 °C to 550 °C of (b). The assignment of IR and Raman modes is provided in Table 1 of the ESI.†

typical stretching vibration modes of C=N and C–N heterocycles.[32] With the increase of the processing temperatures, the position of these peaks also changes. This is another evidence of the structural change in the thermal condensation reaction.

Using the near-infrared (785 nm) light for excitation, the Raman spectra of the g-C_3N_4 products have been recorded. As presented in Fig. 3(b), the fingerprint peaks of melamine at 681 cm^{-1} (triazine ring breathing mode) and 1566 cm^{-1} (–NH_2 bending mode) disappeared in the g-C_3N_4 products.[41,42] Meanwhile, the signature peaks of g-C_3N_4 at 711 cm^{-1} (heptazine ring breathing mode) and 1233 cm^{-1} (stretching vibration modes of C=N and C–N heterocycles) appear.[9] On the other hand, the baseline of the spectra shows a noticeable rise. This may be due to the impurities when the sample is carbonized at high temperatures.

Fig. 3(c) shows the zoomed-in view of the characteristic peaks of melamine and g-C_3N_4 products obtained at 450–550 °C. Clearly, the Raman peaks of g-C_3N_4 emerge gradually along with the increase of preparation temperature. The evolution of Raman spectra shows the composition change of g-C_3N_4 products during thermal condensation. And this is also consistent with the characterization result from FTIR. For a better comparison, Raman and IR peak positions observed in this work and their assignment to the vibrational modes have been listed in detail in ESI Table 1.†

With all the above characterization data, we can clarify the composition of all the products and figure out the condensation mechanism of g-C_3N_4. During the heating process inside the ampoule, melamine forms melem by the polymerization of heptazine units, and melem can further be organized into the g-C_3N_4 network. The efficiency of the reaction is strongly affected by the reaction temperature. When the temperature is below 550 °C, the products will contain both melem and g-C_3N_4 because of incomplete reaction. The percentage of g-C_3N_4 also increases with the increasing reaction temperature. At 550 °C, most of the reagent has transformed into g-C_3N_4. However, carbonization can also occur when the temperature goes higher. Thus, we conclude that the optimal temperature to produce g-C_3N_4 with high purity is ~550 °C.

Emission properties of g-C_3N_4 products

To understand the emission properties of our g-C_3N_4 products, we further studied their photoluminescence (PL) properties. Fig. 4(a) shows the photographs of the multicolor-emission from melamine and the g-C_3N_4 products at the same concentration under UV light illumination (365 nm). We can clearly observe the color variation from blue-violet to green. Meanwhile, the intensity of the emission was enhanced at first and quenched later, indicating that high purity of g-C_3N_4 results in high PL intensity.

The steady-state and transient PL emission spectra have been excited by using a He–Cd laser (325 nm). The normalized photoluminescence spectra in Fig. 4(b) further prove the red shift of the luminescence center when the processing temperature increases from 450 °C to 650 °C. For the melem-rich g-C_3N_4 sample (450 °C), the center of PL spectra is at 369 nm;

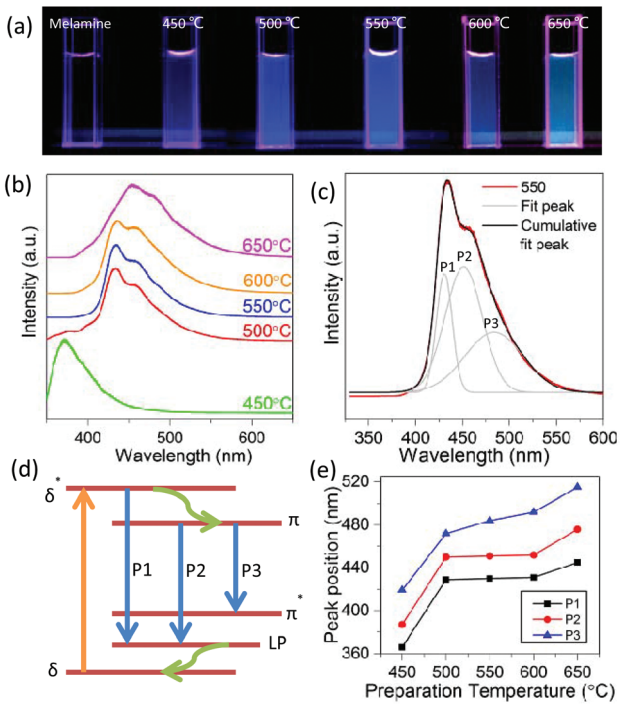

Fig. 4 (a) The photographs of the g-C_3N_4 products in deionized water under UV light (365 nm). (b) The normalized PL emission spectra of the g-C_3N_4 products using 325 nm laser excitation. (c) The Gaussian fitting of PL emission spectra of the 550 °C sample which indicate 3 major PL peaks (P1, P2 and P3). (d) The schematic diagram of the bandgap states of g-C_3N_4. The orange arrow is the excitation, the blue arrows are the emissions and the green arrows are non-radiative transitions. (e) The peak position of P1, P2 and P3 of the g-C_3N_4 products obtained at different temperatures.

for the g-C_3N_4 sample (550 °C), the center of PL spectra is at 430 nm; for the carbonized g-C_3N_4 sample (650 °C), the center of PL spectra is at 455 nm and the peak also becomes broader because of impurities.

Gaussian fitting of the PL peaks helps us obtain a clear understanding of the nature and origin of excitons in the g-C_3N_4 sample. Three major emission centers have been demonstrated in the fitting and decomposition of the emission spectrum of the g-C_3N_4 samples (ESI Fig. S3†). Fig. 4(c) shows the lineshape analysis of the g-C_3N_4 sample prepared at 550 °C, which includes the emission center P1 (429 nm, 2.89 eV), P2 (451 nm, 2.75 eV) and P3 (484 nm, 2.56 eV). According to the previous PL study of g-C_3N_4, the bandgap states of g-C_3N_4 consist of a sp^3 C–N σ band, sp^2 C–N π band and the lone pair (LP) state of the bridge nitride atom (Fig. 4(d)), and the P1, P2 and P3 origin from the 3 different pathways of transitions: π*–π, σ*–LP and π*–LP respectively.[20,43,44] Fig. 4(e) shows the red shift of P1, P2 and P3 with the preparation temperature increase. This red shift can be explained by the extension of the g-C_3N_4 network at higher temperatures. When more heptazine is connected by the amino group, the π states will hybrid into a broad state, causing the bandgap narrowing of the sp^2 C–N clusters.[20]

Low temperature photoluminescence experiments have been carried out. Fig. 5(a–e) show the temperature-dependent PL spectra of the g-C_3N_4 sample obtained from 450 to 650 °C. As the temperature decreases, the features of the PL emission spectra are resolved clearer due to the weaker thermal vibration of atoms at low temperatures. Meanwhile, the peak position also shows the blue shift for about 5–10 nm when the temperature decreases from room temperature to 77 K (Fig. 5(f)). This tunable PL mechanism is mainly attributed to the size reduction of sp^2 C–N clusters when the temperature decreases. A smaller cluster size will result in a larger bandgap and higher probability of the direct transition between the π and π* bands.[43] In addition, the LP valence band shifts in the direction of the π band at low temperatures,[45] so the separation between the LP valence and π* bands will increase and cause a blue shift in the PL emission center. The photoluminescence of carbon nitride in deionized water has also been collected (ESI, Fig. S4†). With water involved, the PL spectra also show a slightly blue shift, which is probably due to the hydrogen-bonding existing in the carbon nitride network, and the LP valence band is affected.

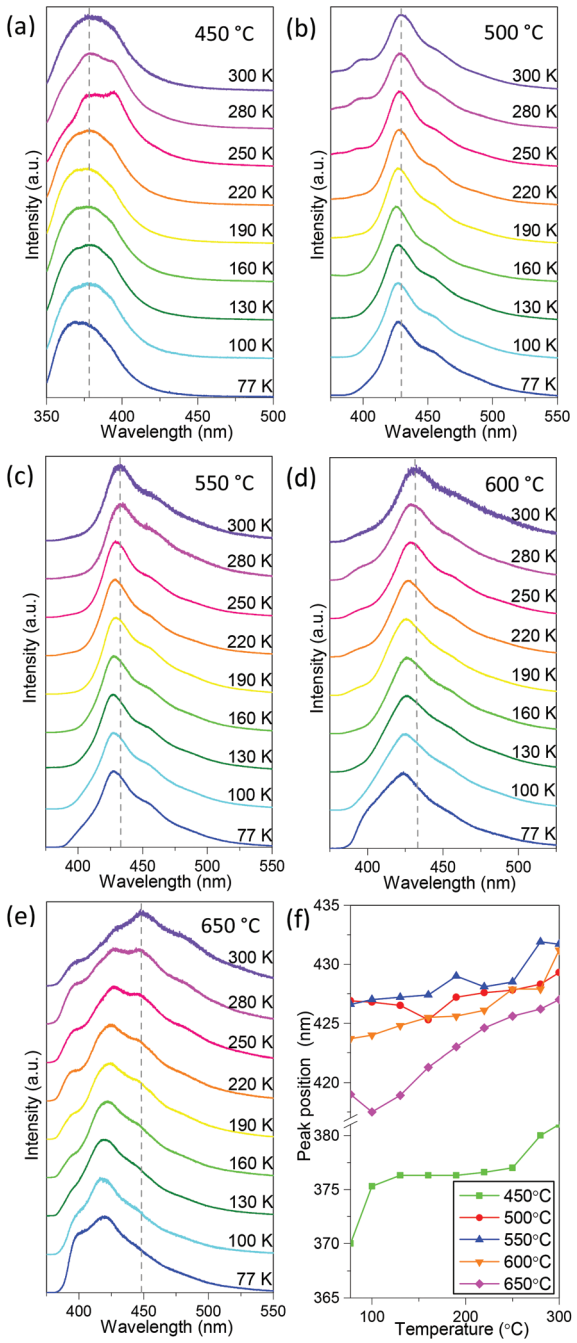

Fig. 5 (a–e) The normalized PL emission spectra of the g-C_3N_4 sample from room temperature (300 K) to liquid nitrogen temperature (77 K). The sample preparation temperature is labelled on the top-right panel. (d) The temperature-dependence of the PL peak position change for the g-C_3N_4 samples obtained at different temperatures.

Photocatalytic degradation using g-C_3N_4 products

To investigate the photocatalytic performance of our g-C_3N_4 products, photocatalytic degradation experiments have been performed. Methylene blue was used as the target for degradation and the degradation efficiencies were evaluated by measuring the peak value of the UV-Vis absorption spectra of methylene blue solution. Fig. 6(a) shows irradiation for different durations of 10 mg L^{-1} methylene blue after photocatalytic degradation by the g-C_3N_4 sample (550 °C) under white light from a solar simulator. It can be clearly seen that the absorbance peak of methylene blue gradually decreased, and nearly went down to 0 after 110 min.

The degradation rates of all the g-C_3N_4 products (450–650 °C) are summarized in Fig. 6(b). With the increasing preparation temperature, the degradation rate of the g-C_3N_4 sample first increased, reached the highest point at 550 °C, and then finally decreased. Judging from the degradation rate, g-C_3N_4 samples with higher purity have higher photocatalytic activity, indicating that g-C_3N_4 has better oxidizability than the by-products of melem or carbonized g-C_3N_4. Moreover, compared with previous literature, our C_3N_4 sample shows a

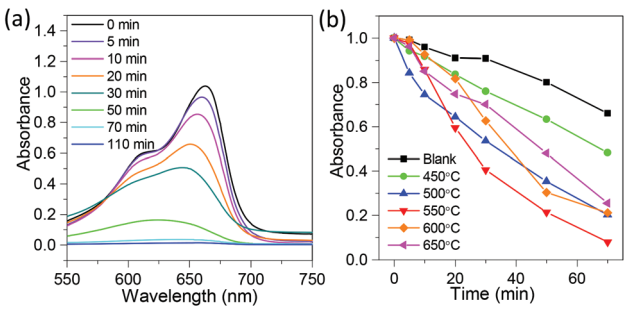

Fig. 6 (a) The absorption spectra of 10 mg L^{-1} methylene blue after photocatalytic degradation by the g-C_3N_4 products synthesized at 550 °C at different time stages. (b) The normalized absorbance of methylene blue with respect to the elapsed time after the start of degradation reaction with the g-C_3N_4 products synthesized at different temperatures.

similar photocatalytic performance to the normal air-heated g-C_3N_4 but with a much higher yield.[4,46]

Conclusions

In conclusion, we successfully prepared a high yield of g-C_3N_4 products using sealed thermal condensation of melamine and investigated the compositional change with the increase of growth temperature. The optical properties and the internal structure of the g-C_3N_4 products have been explored with both FTIR and Raman spectroscopy. Moreover, the PL properties of the g-C_3N_4 products synthesized at different temperatures have been studied. With the increase of synthesis temperature, the carbon nitride products exhibit tunable PL properties. The PL centers vary from blue-violet light region to green light region, which may indicate the optical band gap changes during synthesis. Furthermore, we studied the photocatalytic degradation properties of the g-C_3N_4 products, and concluded that the highest photocatalytic efficiency was obtained at ~550 °C growth temperature.

Acknowledgements

Q. X. gratefully thanks Singapore National Research Foundation *via* a fellowship grant (NRF-RF2009-06), Ministry of Education *via* a tier2 grant (MOE2012-T2-2-086) and a tier1 grant (2013-T1-002-232). The authors thank Dr Emrah Yucelen from FEI for his help during the EELS experiments. Some of the research leading to these results has received funding from the European Union Seventh Framework Program under Grant Agreement 312483 – ESTEEM2 (Integrated Infrastructure Initiative – I3). AZ acknowledges the German DAAD scholarship program.

Notes and references

1 Y. Wang, X. Wang and M. Antonietti, *Angew. Chem., Int. Ed.*, 2012, **51**, 68–89.
2 K. Maeda, X. Wang, Y. Nishihara, D. Lu, M. Antonietti and K. Domen, *J. Phys. Chem. C*, 2009, **113**, 4940–4947.
3 X. Wang, K. Maeda, A. Thomas, K. Takanabe, G. Xin, J. M. Carlsson, K. Domen and M. Antonietti, *Nat. Mater.*, 2008, **8**, 76–80.
4 S. Yan, Z. Li and Z. Zou, *Langmuir*, 2010, **26**, 3894–3901.
5 J. Liu, Y. Liu, N. Liu, Y. Han, X. Zhang, H. Huang, Y. Lifshitz, S.-T. Lee, J. Zhong and Z. Kang, *Science*, 2015, **347**, 970–974.
6 E. G. Gillan, *Chem. Mater.*, 2000, **12**, 3906–3912.
7 Y. Zheng, J. Liu, J. Liang, M. Jaroniec and S. Z. Qiao, *Energy Environ. Sci.*, 2012, **5**, 6717–6731.
8 M. L. Cohen, *Mater. Sci. Eng., A*, 1996, **209**, 1–4.
9 S. Tonda, S. Kumar, S. Kandula and V. Shanker, *J. Mater. Chem. A*, 2014, **2**, 6772–6780.
10 H. Yao and W. Ching, *Phys. Rev. B: Condens. Matter*, 1994, **50**, 11231.
11 Y. Xu, M. Xie, S. Huang, H. Xu, H. Ji, J. Xia, Y. Li and H. Li, *RSC Adv.*, 2015, **5**, 26281–26290.
12 S. Yan, Z. Li and Z. Zou, *Langmuir*, 2009, **25**, 10397–10401.
13 S. Wang, C. Li, T. Wang, P. Zhang, A. Li and J. Gong, *J. Mater. Chem. A*, 2014, **2**, 2885–2890.
14 W. Wang, J. C. Yu, D. Xia, P. K. Wong and Y. Li, *Environ. Sci. Technol.*, 2013, **47**, 8724–8732.
15 L. Maya, D. R. Cole and E. W. Hagaman, *J. Am. Ceram. Soc.*, 1991, **74**, 1686–1688.
16 M. Lei, H. Zhao, H. Yang, B. Song and W. Tang, *J. Eur. Ceram. Soc.*, 2008, **28**, 1671–1677.
17 X. Wang, K. Maeda, X. Chen, K. Takanabe, K. Domen, Y. Hou, X. Fu and M. Antonietti, *J. Am. Chem. Soc.*, 2009, **131**, 1680–1681.
18 A. B. Jorge, D. J. Martin, M. T. Dhanoa, A. S. Rahman, N. Makwana, J. Tang, A. Sella, F. Corà, S. Firth and J. A. Darr, *J. Phys. Chem. C*, 2013, **117**, 7178–7185.
19 G. Liu, P. Niu, C. Sun, S. C. Smith, Z. Chen, G. Q. Lu and H.-M. Cheng, *J. Am. Chem. Soc.*, 2010, **132**, 11642–11648.
20 Y. Zhang, Q. Pan, G. Chai, M. Liang, G. Dong, Q. Zhang and J. Qiu, *Sci. Rep.*, 2013, **3**.
21 H. Zhang and A. Yu, *J. Phys. Chem. C*, 2014, **118**, 11628–11635.
22 S. Muhl and J. M. Mendez, *Diamond Relat. Mater.*, 1999, **8**, 1809–1830.
23 T. Komatsu, *J. Mater. Chem.*, 2001, **11**, 799–801.
24 Y. Zhao, D. Yu, O. Yanagisawa, K. Matsugi and Y. Tian, *Diamond Relat. Mater.*, 2005, **14**, 1700–1704.
25 J. Xu, Y. Li, S. Peng, G. Lu and S. Li, *Phys. Chem. Chem. Phys.*, 2013, **15**, 7657–7665.
26 B. Jürgens, E. Irran, J. Senker, P. Kroll, H. Müller and W. Schnick, *J. Am. Chem. Soc.*, 2003, **125**, 10288–10300.
27 Q. Guo, Y. Xie, X. Wang, S. Lv, T. Hou and X. Liu, *Chem. Phys. Lett.*, 2003, **380**, 84–87.
28 A. Thomas, A. Fischer, F. Goettmann, M. Antonietti, J.-O. Müller, R. Schlögl and J. M. Carlsson, *J. Mater. Chem.*, 2008, **18**, 4893–4908.
29 H. Ma, X. Jia, L. Chen, P. Zhu, W. Guo, X. Guo, Y. Wang, S. Li, G. Zou and G. Zhang, *J. Phys.: Condens. Matter*, 2002, **14**, 11269.
30 J. Yang, X. Wu, X. Li, Y. Liu, M. Gao, X. Liu, L. Kong and S. Yang, *Appl. Phys. A*, 2011, **105**, 161–166.
31 H. Xu, J. Yan, X. She, L. Xu, J. Xia, Y. Xu, Y. Song, L. Huang and H. Li, *Nanoscale*, 2014, **6**, 1406–1415.
32 V. N. Khabashesku, J. L. Zimmerman and J. L. Margrave, *Chem. Mater.*, 2000, **12**, 3264–3270.
33 C. Ronning, H. Feldermann, R. Merk, H. Hofsäss, P. Reinke and J.-U. Thiele, *Phys. Rev. B: Condens. Matter*, 1998, **58**, 2207.
34 H. Estrade-Szwarckopf, *Carbon*, 2004, **42**, 1713–1721.
35 Y. Li, J. Zhang, Q. Wang, Y. Jin, D. Huang, Q. Cui and G. Zou, *J. Phys. Chem. B*, 2010, **114**, 9429–9434.
36 Y.-A. Li, S. Xu, H.-S. Li and W.-Y. Luo, *J. Mater. Sci. Lett.*, 1998, **17**, 31–35.
37 N. Daems, X. Sheng, I. F. Vankelecom and P. P. Pescarmona, *J. Mater. Chem. A*, 2014, **2**, 4085–4110.

38 Q. Guo, Y. Xie, X. Wang, S. Zhang, T. Hou and S. Lv, *Chem. Commun.*, 2004, 26–27.
39 M. Jelínek, J. Zemek, M. Trchova, V. Vorlíček, J. Lančok, R. Tomov and M. Šimečková, *Thin Solid Films*, 2000, **366**, 69–76.
40 J. Wei, P. Hing and Z. Mo, *Surf. Interface Anal.*, 1999, **28**, 208–211.
41 P. V. Zinin, L.-C. Ming, S. K. Sharma, V. N. Khabashesku, X. Liu, S. Hong, S. Endo and T. Acosta, *Chem. Phys. Lett.*, 2009, **472**, 69–73.
42 R. Meier, J. Maple, M.-J. Hwang and A. Hagler, *J. Phys. Chem.*, 1995, **99**, 5445–5456.
43 B. Wang, Q. Cheng, L. Wang, K. Zheng and K. Ostrikov, *Carbon*, 2012, **50**, 3561–3571.
44 B. Wang, Q. Cheng, Y. Chen and K. Ostrikov, *J. Appl. Phys.*, 2011, **110**, 054323.
45 G. Fanchini, A. Tagliaferro, N. Conway and C. Godet, *Phys. Rev. B: Condens. Matter*, 2002, **66**, 195415.
46 L. Song, S. Zhang, X. Wu and Q. Wei, *Chem. Eng. J.*, 2012, **184**, 256–260.